On the systematics of rheological measurements of gas fluidized grains

Marlo Kunzner[1,2,*], *Matthias* Sperl[1,2,**], and *Jan P.* Gabriel[1,***]

[1]Institut für Materialphysik im Weltraum, Deutsches Zentrum für Luft- und Raumfahrt (DLR), 51170 Cologne, Germany
[2]Institute for Theoretical Physics, University of Cologne, Zülpicher Straße 77, 50937 Cologne, Germany

Abstract. There have been many attempts to characterize the flow behavior of fluidized and non-fluidized granular particles [1–4]. The well-known Geldart classification [5] divides granular particles by their fluidization characteristics and the rheology of air-fluidized granular media has been recently investigated both experimentally and theoretically [4, 6], considering the fluidized bed as a homogeneous medium. We propose a measurement protocol for accounting for the abundant effects which can occur in a fluidized bed when using a rheometer, using Polystyrene (PS) particles with a diameter of 140 µm. We observe that the system becomes more viscous over time as charges accumulate.

1 Introduction

The reasons why granular material can flow and said flow's characteristics are poorly understood [1, 4, 7]. While many analogies to colloids have been made granular matter is vastly different from these systems due to a variety of effects, such as electrostatics, friction and not to mention gravity, although the volume fractions of granular matter and colloids can comparable [1, 8, 9]. It is therefore important to be able to account for the aforementioned effects during a measurement and estimate or determine their effects on a system. Therefore this work will focus mostly on the experimental approach to characterizing flow behavior of granular matter with a rheometer and the expansion of the observable system characteristics.

2 Experimental Approach

A strain-controlled Anton-Paar rheometer MCR 102 is used with the powder cell expansion as a sample container, in a Couette-Geometry set-up [10]. The dimensions and a schematic are given in Fig. 1. The cell itself has a radius, r, of 25 mm, the measurement geometry or cylinder has a radius of 10.5 mm. The cell is sealed by a particle filter at the top to prevent the escape of particles while allowing air flow. The cell is operated at ambient conditions. Initially a pressure measurement dependent on gas flow is taken for an empty sample cell. Following this, Polystyrene (PS) particles with a diameter of 140 μm with a total weight of 61 g are filled into the sample cell, and are fluidized by dry pressurized air with adjustable volumetric flow rate ($\dot{Q}$) from the bottom. The flow rate is decreased in two different linear sweeps. It begins at a very high flow rate, of 3.3 L/min, in relation to the pressure drop flow rate, which is elaborated upon later (Sec. 3) and represents the minimum flow rate necessary to break apart particle contacts, after which there are 10 decrements of 0.23 L/min, down to slightly above the pressure drop flow rate. Following this the flow rates around the pressure drop are measured in five steps of 0.1 L/min, after which a measurement for no fluidization is taken. In total, 16 flow rate measurements will be taken from this series. While the serrated cylinder of the Couette cell measures the torque (τ) at determined rotational rate (Ω), a camera records the height of the powder bed and thereby gives insights on the global volume fraction, φ_g [10]. The torque at the inner cylinder can be used to calculate a shear stress, σ, according to Eq. 1.

$$\sigma = \tau / \pi L R_i^2 \tag{1}$$

Here L is the length of the geometry of 38 mm and R_i is the radius of the geometry, shown in Fig. 1.

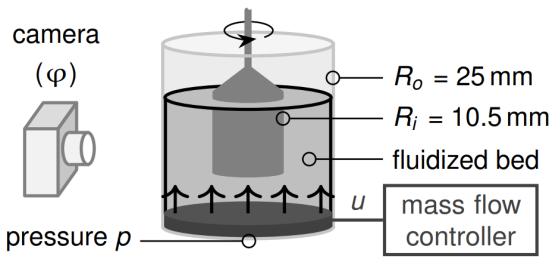

Figure 1. A schematic of the measurement set-up. Reprinted with permission from D'Angelo [4]. Gas is forced through a porous glass frit, the bottom black plate, thereby lifting up the grains, surrounding the cylindrical measurement geometry with a radius of 10.5 *mm*, shown as gray continuous mass. The sample cell itself is 25 *mm* in radius has a mass flow controller, to adjust the flow rate ($\dot{Q}$), and a pressure sensor installed to monitor the bed's properties. Additionally a camera is used to record the volume fraction φ.

*e-mail: marlo.kunzner@dlr.de
**e-mail: matthias.sperl@dlr.de
***e-mail: jan.gabriel@dlr.de

Since many rheological theories, such as Mode-Coupling Theory or the Maxwell-model, are only meaningfully fitted if a system is in thermal equilibrium or a steady-state. We want to explore how close our system is to a steady-state [11–13].

In order to determine the point fluidization onset the experiments begin with a pressure drop measurement [2, 14]. This measurement is the same as the aforementioned pressure depending on flow rate measurement for the empty cell. The flow rate starts at 2.5 L/min and decreases to 0.05 L/min in 1600 steps, since the flow rate decreases this is called down sweep. Following this there is a small deaeration period of 20 seconds. Lastly the flow rate is increased from 0.05 L/min in 1600 steps, during the upsweep. The pressure sweeps from the filled cell are deducted by the empty cell's sweeps. Afterwards the system is sheared while the camera records the global volume fraction at different fluidization rates. There is a 10 second video recording for each $\dot{Q}$ and Ω combination with 18 different Ω values and 16 flow rates, this way we are able to calculate an average bed height for each point.

Following this, another pressure drop measurement is taken. Next up is a method for determining the closeness to the steady-state: The rheometer measures at a fixed volumetric flow rate and rotation rate for a little over an hour while recording the torque value for 1000 data points.

A third pressure drop is recorded, after which the flow curves are recorded. The flow curve measurements consist of 38 data points per flow rate, spaced equidistant across slightly over 5 decades. The limits of $\Omega = 10^{-4}$ and 13.3 Hz are given by the rheometer model. Each data point is recorded for up to a maximum duration of 240 seconds. The flow curves need at least 5 repetitions without interruption to determine if the system still changes. Once the threshold of 5 repetitions has been reached or exceeded, the measurement can be concluded by recording a final pressure drop curve. The supplementary material provides further information on the experiment procedure.

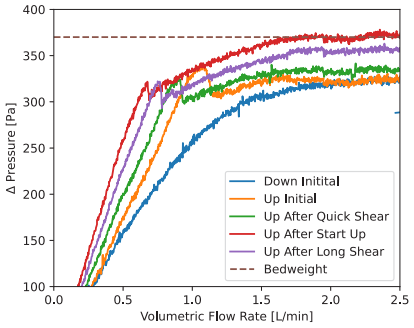

Figure 2. Pressure drop curves for 140μm PS particles plotted as pressure difference versus flow rate. The dashed line represents the maximum pressure difference caused by the weight of the sample. The different colors represent different chronologic times in the experiment. A change in height of the pressure difference and minimum flow rate until the pressure overshoot is visible.

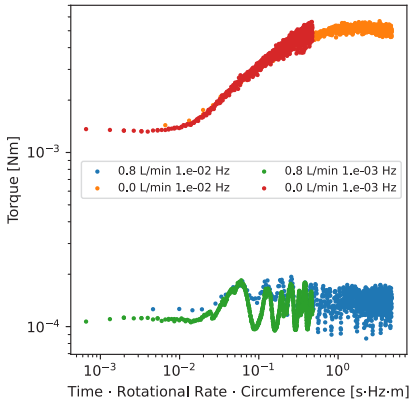

Figure 3. A start up curve plot for 140 μm PS particles showing torque versus normalized rotation length, recorded at $\Omega = 10^{-2}$ and 10^{-3} Hz and flow rates of 0.0 and 0.8 L/min, respectively.

3 Results and Discussion

Fig. 2 shows all the pressure drop measurements, with the dashed line indicating the pressure at which the plateau should be, given by the weight of the sample according to Eq. 2. Here Δp is the pressure difference between filled and empty cell, m the mass, g the gravitational constant and R_0, R_i the outer and inner radius respectively.

$$\Delta p = m \cdot g/(\pi \cdot (R_0^2 - R_i^2) \tag{2}$$

[2, 4]. Only the initial measurement shows both the up and down flow rate sweep. For the rest, only the upsweep is shown to highlight the pressure overshoot. The shift in position of the overshoot and height of the plateau is clearly visible, indicating a change in the properties of the system. A higher $\dot{Q}$ means a higher energy input, since the particles need more energy to be broken apart. For the initial pressure drop measurement the plateau does not reach the dashed line, implying that the mass is effectively smaller than 61 g, as all other terms in the pressure drop equation, Eq. 2, are constant. The height of the drop from the peak of a pressure overshoot peak to the downwards sweep, can be seen as a measure for cohesive forces, which also change. The cohesive forces involved are most likely a mixture of electrostatics, via tribo-charging and Van der Waals forces, more specifically the London component [14, 15].

The Start-Up curves for two different flow rates are shown in Fig. 3. The torque is plotted versus the normalized distance the inner cylinder rotated. A plateau is reached for $\Omega = 10^{-2}$ Hz, indicating that a steady state is reached, $\Omega = 10^{-3}$ Hz however is not in steady-state yet. The length or time until the plateau is reached can be used to determine the duration necessary to reach steady-state flow curve points, thereby the experimentalist gains insights on how representative each future flow curve is. The oscillations visible for a flow rate of 0.8 L/min are caused by the resolution limits of the rheometer, as the oscillations decrease with increasing measurement time per data point.

As the camera records the entire duration of the quick

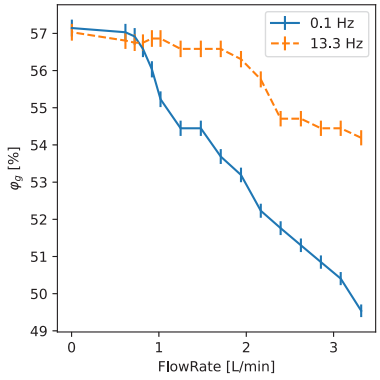

Figure 4. Evolution of the global volume fraction recorded with a camera dependent on flow rate and rotational rates. The blue line depicts rotational rates lower than 1 Hz, whereas the dashed orange line shows a rotation rate of 13.3 Hz.

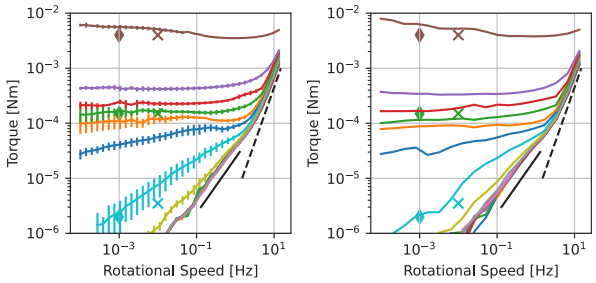

Figure 5. Flow curves in steady state, on the left, and not in steady state on the right. Torque, τ, vs rotational rate, Ω, of the inner cylinder. The left curve is the mean value of data averaged over long shear 3 sweeps. The right curve is the quick sweep with 10 seconds per data point. The diamonds and x-es indicate the recorded steady state values, by the start-up curves. They are taken at 0, 0.8 and 1.3 L/min, respectively. The dashed black line indicates a slope of 2, while the black line indicates a slope of 1.

shear sweep, insights on the global packing fraction dependent on Ω are given. Fig. 4 shows the behavior for the high shear rate (>1 Hz) or Bagnold regime and the lower shear rate regime (<0.5 Hz), called Newtonian here [3, 16]. Especially for high flow rates the difference between high and low Ω becomes obvious, as the differences reach values up to 4 %. We suspect that it by the power input of shear and fludiziation respectively. Meaning that rotational rates lower than 0.1 Hz should show the same behavior as 0.1 Hz, as the energy input by shear is negligible in comparison to the input by the gas flow. This is further supported by the φ_g of high rotational rates showing no apparent change for almost up to 2 L/min, after which the energy input of the gas flow dominates over shear power. This can also be viewed as the bubbles in the fluidized bed being destroyed by the strong shear, thereby the system does not expand as much. Additionally, the beginning of the decrease of φ_g stirred by low Ω aligns with the values recorded for the position of the pressure overshoot. These results lead us to believe that the volume fraction is a function of Ω and $\dot{Q}$ ($\varphi_g(\Omega, \dot{Q})$). We furthermore assume that this can be viewed as a measure of the heterogeneity in the system.

Two noteworthy flow curves are shown in Fig. 5. The left plot shows a steady-state sweep which has been averaged 3 times and the standard deviation (σ_{STD}) is plotted as an error bar, whereas the right shows the non-steady-state case. The flow curves possess a slope of almost 2 for high Ω (>1 Hz), where the shear stress is proportional to the granular temperature, this is an indication of an on-set the aforementioned Bagnold regime [3, 16, 17]. Granular matter is often viewed as hard spheres where no inherent relaxation timescale for the particles exists, implying that the only timescale is the shear. This leads to the the fact that the collision frequency is proportional to Ω^2, or the aforementioned granular temperature [4]. However the limits of the rheometer make it impossible to collect any higher Ω, thereby denying us certainty, even though the point of on-set agrees with literature [4]. Fig. 5 shows a plateau for Ω < 1, which looks like shear thinning or solid-like for some

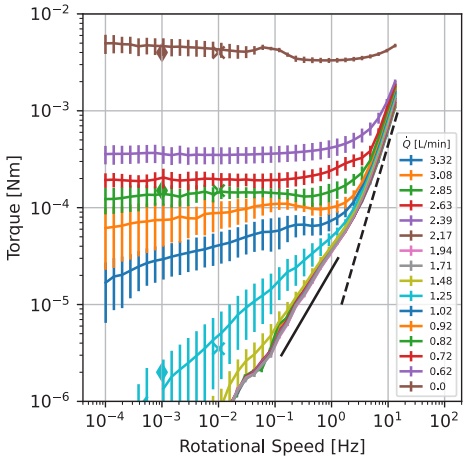

Figure 6. Flow curve in steady state. Mean values of torque versus rotational rate of the inner cylinder. The data is averaged over 7 repetitions. The error bars are the σ_{STD} from the mean. The diamonds and x-es indicate the recorded steady state values, by the start-up curves. They are taken at 0, 0.8 and 1.3 L/min, respectively. The dashed black line indicates a slope of 2, while the black line indicates a slope of 1.

of the flow curves with low excitation. The length of the plateau depends on the energy supplied by the air. When the agitation is strong enough, the system shows a slope of 1, looking like Newtonian flow behavior. The onset of this flow behavior can be found between 10^{-4} and 1 Hz, as seen in the orange to olive curve. It is worth mentioning that the flow curve for no agitation and the ones close to the flow rate necessary for the pressure overshoot look non-monotonic, as seen in other literature and attributed to shear bands [4, 18].

As $\tau \propto \sigma$ the intercept of each plateau with the ordinate can be seen as a dynamic yield stress, which changes with varying flow rate [18]. The curves share characteristics of previous work on gas-fluidized beds but also

vibro-fluidized beds [4, 18, 19]. For example, in the non-monotonic flow curve for no agitation, a dynamic yield stress which differs from the supposed static one, and a shear thinning plateau between the slope of 1 and 2 fit previous observations very well [18]. The slopes smaller than 2 for $\Omega > 1$ Hz, as observed by Wortel, can also be seen in our graphs (See Supplement). In comparison between the two curves the absolute torque value is shifted by a factor of roughly 1.3. This however is not enough to properly express a change in the system.
Therefore Fig. 6. shows data averaged over 7 sweeps including the initial one and the error bars are the σ_{STD} again. It is clearly visible that the σ_{STD} is smaller and that the absolute value of the mean increases from Fig. 6 to Fig. 5; showing that something changed in the system which is not caused by being out of equilibrium. An increase in torque or shear stress can indicate a more cohesive system. It also shows that the system stops changing after a while, as the mean value remains constant and the σ_{STD} decreases by adding sweeps which are chronologically in the back. Fig. 6 also has mean values with align better with the steady state values, prompting us to believe that it is necessary to take steady state recordings after the shear sweeps too.

4 Conclusion

The volume fraction decreases with the decreasing ratio of energy supplied by shear with respect to airflow. We conclude which parts of a flow curve can be seen as in steady state, and which ones are still in a transient state, by using start-up curves. The recorded torque of the flow curves increases up to a saturation level over time. This behavior seems to indicate that the systems gradually become more resistant to flow, likely to the accumulation of charge. We can rule out that the system has not reached an equilibrium with the shear energy or a steady-state in that regard, meaning that properties of the system itself evolve. Further expansions of the protocol will include steady-state measurements at the beginning and end of each measurement.

5 Acknowledgments

The authors thank for discussion and support Christopher Mayo, Martin J. Uttendorfer, Karsten Tell, Elisabeth Bujnoch and, Felicitas Bujnoch.

References

[1] B. Andreotti, Y. Forterre, O. Pouliquen, Granular media: between fluid and solid (Cambridge University Press, 2013)
[2] J. Gottschalk, Rheological study of loosened bulk granular materials, Part. Part. Syst. Charact. **3**, 168 (1986).
[3] R.A. Bagnold, Experiments on a gravity-free dispersion of large solid spheres in a newtonian fluid under shear, Proc. Roy. Soc. **225**, 49 (1954).
[4] O. D'Angelo, A. Shetty, M. Sperl, W.T. Kranz, The manifold rheology of fluidized granular media, arXiv preprint arXiv:2309.00413 (2023).
[5] D. Geldart, Types of gas fluidization, Powder Technol. **7**, 285 (1973).
[6] O. D'Angelo, M. Sperl, W.T. Kranz, Rheological regimes in agitated granular media under shear, Phys. Rev. Lett. **134**, 148202 (2025).
[7] M. Kunzner, C. Mayo, M. Sperl, J.P. Gabriel, The dynamics in vibro-fluidized beds: A diffusing wave spectroscopy study, arXiv preprint arXiv:2503.00517 (2025).
[8] F.P. Bowden, D. Tabor, Friction: an introduction to tribology (R.E. Krieger Publishing Company, 1973)
[9] G.L. Hunter, E.R. Weeks, The physics of the colloidal glass transition, Rep. Prog. Phys. **75**, 066501 (2012).
[10] V. Francia, L.A.A. Yahia, R. Ocone, A. Ozel, From quasi-static to intermediate regimes in shear cell devices: Theory and characterisation, KONA Powder Part. J. **38**, 3 (2021).
[11] M. Fuchs, M.E. Cates, A mode coupling theory for brownian particles in homogeneous steady shear flow, J. Rheol. **53**, 957 (2009).
[12] E.M. Furst, T.M. Squires, Microrheology (Oxford University Press, 2017)
[13] M. Sperl, W.T. Kranz, A. Zippelius, Single-particle dynamics in dense granular fluids under driving, Europhys. Lett. **98**, 28001 (2012).
[14] M. Baerns, Effect of interparticle adhesive forces on fluidization of fine particles, Ind. Eng. Chem. Res. **5**, 508 (1966).
[15] A. Schella, S. Herminghaus, M. Schröter, Influence of humidity on tribo-electric charging and segregation in shaken granular media, Soft Matter **13**, 394 (2017).
[16] G. Lois, A. Lemaître, J.M. Carlson, Numerical tests of constitutive laws for dense granular flows, Phys. Rev. E **72**, 051303 (2005).
[17] I. Goldhirsch, Introduction to granular temperature, Powder Technol. **182**, 130 (2008).
[18] J.A. Dijksman, G.H. Wortel, L.T. Van Dellen, O. Dauchot, M. Van Hecke, Jamming, yielding, and rheology of weakly vibrated granular media, Phys. Rev. Lett. **107**, 108303 (2011).
[19] G. Wortel, O. Dauchot, M. van Hecke, Criticality in vibrated frictional flows at a finite strain rate, Phys. Rev. Lett. **117**, 198002 (2016).